The Journal of Experimental Biology 210, 1362-1377
Published by The Company of Biologists 2007
doi:10.1242/jeb.02746

The aerodynamic benefit of wing–wing interaction depends on stroke trajectory in flapping insect wings

Fritz-Olaf Lehmann* and Simon Pick

BioFuture Research Group, Institute of Neurobiology, University of Ulm, Albert-Einstein-Allee 11, 89081 Ulm, Germany

*Author for correspondence (e-mail: fritz.lehmann@uni-ulm.de)

Accepted 12 February 2007

Summary

Flying insects may enhance their flight force production by contralateral wing interaction during dorsal stroke reversal ('clap-and-fling'). In this study, we explored the forces and moments due to clap-and-fling at various wing tip trajectories, employing a dynamically scaled electromechanical flapping device. The 17 tested bio-inspired kinematic patterns were identical in stroke amplitude, stroke frequency and angle of attack with respect to the horizontal stroke plane but varied in heaving motion. Clap-and-fling induced vertical force augmentation significantly decreased with increasing vertical force production averaged over the entire stroke cycle, whereas total force augmentation was independent from changes in force produced by a single wing. Vertical force augmentation was also largely independent of forces produced due to wing rotation at the stroke reversals, the sum of rotational circulation and wake capture force. We obtained maximum (17.4%) and minimum (1.4%) vertical force augmentation in two types of figure-eight stroke kinematics whereby rate and direction of heaving motion during fling may explain 58% of the variance in vertical force augmentation. This finding suggests that vertical wing motion distinctly alters the flow regime at the beginning of the downstroke. Using an analytical model, we determined pitching moments acting on an imaginary body of the flapping device from the measured time course of forces, the changes in length of the force vector's moment arm, the position of the centre of mass and body angle. The data show that pitching moments are largely independent from mean vertical force; however, clap-and-fling reinforces mean pitching moments by approximately 21%, compared to the moments produced by a single flapping wing. Pitching moments due to clap-and-fling significantly increase with increasing vertical force augmentation and produce nose-down moments in most of the tested patterns. The analytical model, however, shows that algebraic sign and magnitude of these moments may vary distinctly depending on both body angle and the distance between the wing hinge and the animal's centre of mass. Altogether, the data suggest that the benefit of clap-and-fling wing beat for vertical force enhancement and pitch balance may change with changing heaving motion and thus wing tip trajectory during manoeuvring flight. We hypothesize that these dependencies may have shaped the evolution of wing kinematics in insects that are limited by aerodynamic lift rather than by mechanical power of their flight musculature.

Key words: clap-and-fling, wing–wake interaction, wing tip trajectory, heaving motion, analytical modelling, robotic wing, force control, insect flight.

Introduction

Throughout the past decades, the mechanisms of aerodynamic force production and lift augmentation in flapping insect wings have been the subject of many thorough analytical and experimental investigations (for reviews, see Lehmann, 2004; Sane, 2003). This research started back in the 1970s, when Weis-Fogh described a novel pattern of wing motion occurring at dorsal stroke reversal in the tiny chalcid wasp *Encarsia formosa* – the clap-and-fling (Weis-Fogh, 1973). During the clap phase of the stroke, the insect brings the leading edges of both wings together, while pronating them until the gap disappears and the wings are parallel in close apposition. The downstroke of the stroke cycle is then initiated by the fling phase in which the wings pronate about their trailing edge, creating a growing gap as the leading edges pull apart. Marden's classical behavioural experiments on the load-lifting capacity of various insects (Marden, 1987) showed that insects generate approximately 25% more aerodynamic lift per unit flight muscle (79.2 N kg^{-1} mean value) when they clap-and-fling than insects using conventional wing kinematics (59.4 N kg^{-1} mean value), although these values were based solely on an estimate of induced power requirements for flight.

Several studies have previously examined the clap-and-fling and its underlying fluid dynamic phenomena, using both analytical methods (Edwards and Cheng, 1982; Ellington, 1975; Lighthill, 1973) and physical models (Bennett, 1977; Maxworthy, 1979; Spedding and Maxworthy, 1986; Sunada et al., 1993). Numerical simulations on the entire clap-and-fling sequence have been presented (Sun and Yu, 2003), and the time course of lift enhancement of clap-and-fling modelled in two dimensions across a wide range of Reynolds numbers (Miller and Peskin, 2005). A recent experimental study on the clap-and-fling in a three-dimensional (3D) stroke pattern has verified these theoretical predictions and highlighted a complex diversity of aerodynamic mechanisms involved in clap-and-fling lift augmentation, such as a pronounced attenuation of forces during the clap phase of the stroke cycle (Lehmann et al., 2005).

The clap-and-fling and its subtle variations in the precise motion of the wings has already been investigated in many species of insects, including bush cricket and mantis (Brackenbury, 1990; Brackenbury, 1991b), locust (Cooter and Baker, 1977), various species of butterflies (Brackenbury, 1991a; Brodsky, 1991; Dalton, 1975; Ellington, 1984a), and tethered flying *Drosophila* (Götz, 1987; Lehmann, 1994). A partial or near clap-and-fling, during which the wings approach at the dorsal stroke reversal without physically touching each other, was discovered in the white butterfly *Pieris barssicae*, the bluebottle *Calliphora vicina* and the flour moth *Ephista* (Ellington, 1984a; Ennos, 1989). Large insects employ clap-and-fling kinematics while carrying loads (Marden, 1987), or performing power-demanding flight turns (Cooter and Baker, 1977). Consequently, Ellington suggested that the lacewing *Chrysopa carnea* uses clap-and-fling not only for lift augmentation, but also for stability and flight control (Ellington, 1984a). This view on the clap-and-fling is supported by several other experimental studies. First, tethered flying *Drosophila* exhibit an ipsi-contralateral asymmetry in wing motion during clap-and-fling in response to the presentation of optomotor stimuli (Götz, 1987; Zanker, 1990b). Second, concomitant measurements of air velocities during optomotor stimulation in the fruit fly revealed that the wake behind the dorsal stroke reversal is deflected towards the inner side of the flight curve, supposedly producing a turning moment around the animal's vertical yaw axis (Lehmann, 1994). Third, an electrophysiological study on the second basalare control muscle M.b2 in *Drosophila* demonstrated that the fly may actively delay pronation of the wing on the inner side of a visually induced turn during dorsal stroke reversal by as much as 0.2 ms (Lehmann, 1994). The latter value corresponds to approximately 4% of the 5 ms stroke cycle period in this species. Moreover, recent high-speed video recordings of freely flying fruit flies have shown that this insect occasionally employs a clap-and-fling motion during free flight (Ennos, 1989; Fry et al., 2003), but frequently exhibits a complete clap-and-fling when flown under tethered conditions (Götz, 1987; Lehmann, 1994; Vogel, 1966; Zanker, 1990a).

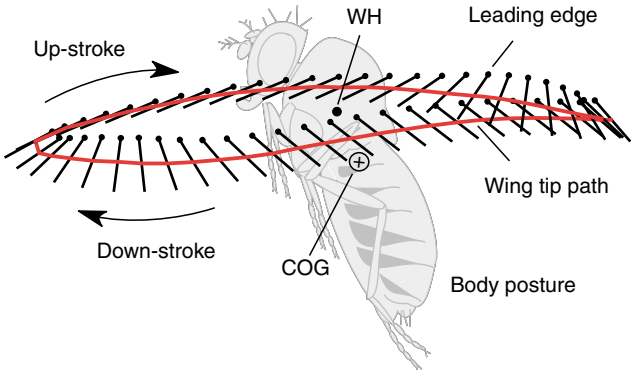

Fig. 1. Pear-shaped wing tip trajectory (red) during wing flapping of a tethered fruit fly *Drosophila melanogaster*. Black dot indicates wing insertion point (WH) on the insect body; circled cross shows the position of the centre of body mass (COG) at the transition between thorax and abdomen. Superimposed body posture was reconstructed from free flight experiments. *Drosophila* wing trajectory is most similar to kinematic pattern D in Fig. 2.

In comparison to the more stereotyped clap-and-fling manoeuvre, the trajectories described by the wing tip (stroke shape) in flying insects are remarkably diverse. Major stroke shapes cover oval, figure-eight and pear-shaped trajectories, including various combinations of those patterns. A simple oval shape has been found in the ladybird *Coccinella 7-punctata*, the hover-fly *Episyrphus balteatus*, the bumblebee *Bombus hortorum*, the lacewing *Sisyra fuscata*, for the forewing motion of brown lacewing *Hemerobius simulans* and in the alderfly *Sialis morio*, whereas figure-eight shapes have been reported for the honey bee *Apis mellifera*, the mayfly *Ephemera vulgata*, the stonefly *Isoptena serricornis*, the scorpionfly *Panorpa communis* and various other insects (Brodsky, 1994; Ellington, 1984a; Magnan, 1934; Marey, 1873). More complex trajectories ('double-eight') have been reconstructed for wing motion in the tethered blow fly *Calliphora erythrocephala* and a beetle *Megopis* sp. (Nachtigall, 1966; Schneider, 1980). Elaborate studies on stroke shape have moreover shown that flies in particular may rapidly change stroke trajectories during steering behaviour. The blowfly, for example, changes its wing trajectory from a figure-eight pattern when the basalare control muscles M.b1 and M.b2 are inactive, to a more oval shape pattern, when these muscles are activated by the nervous system (Balint and Dickinson, 2001; Tu and Dickinson, 1996). Other studies demonstrated changes of a pear-shaped stroke during optomotor stimulation of tethered flying fruit flies *Drosophila*, however, compared to the blowfly these changes were comparatively small and largely limited to the upward portion of the stroke cycle (Lehmann, 1994; Zanker, 1990b) (Fig. 1). Although a previous study on stroke shape using a robotic wing has already highlighted some of the aerodynamic consequences of those changes at intermediate Reynolds numbers, none of these studies have explored how forces and moments change with changing

stroke shape and thus vertical heaving motion of the wings during clap-and-fling wing beat (Sane and Dickinson, 2001). Which wing tip trajectory potentially offers the maximum benefit for force augmentation, flight control and efficiency due to dorsal wing–wing interaction in an insect remains an open question.

Consequently, in this study we explored the forces and moments produced by dorsal wing–wing interaction (clap-and-fling) using 17 gross kinematic patterns in a dynamically scaled two-winged electromechanical flapper. This mechanical device is equipped with model wings shaped like the wings of the small fruit fly *Drosophila*, and permits measurements of the time course of vertical and horizontal force throughout the entire stroke cycle while manipulating the kinematics of wing motion during wing translation. We evaluated the relationships between stroke shape due to systematic changes in the wing's heaving motion and the aerodynamic effect of wing–wing interaction by estimating the augmentation of total flight force, vertical and horizontal force with respect to the performance of a single flapping wing. Incorporating estimates of the moment arm for turning moments, we derived changes in pitching moment on an imaginary insect body both at various kinematic flapping conditions and also a variety of morphological designs of the artificial insect body.

Materials and methods

To assess the gross effects of clap-and-fling wing beat on the production of forces and moments in flapping insect wings experimentally, we modelled clap-and-fling during hovering flight using a dynamically scaled electromechanical model. This method has already been published elsewhere in greater detail, so we provide only a brief description here (Dickinson et al., 1999; Maybury and Lehmann, 2004). We used two computer-controlled dynamically scaled Plexiglas^{TM} wings (left and right wing) programmed to flap back and forth in prescribed kinematic patterns. One wing was equipped with a 2-DoF force transducer that measured forces perpendicular and parallel to the wing in the spanwise direction. From the measured forces and the angular position of the wing throughout the stroke cycle, we reconstructed vertical and horizontal force using custom software routines in Matlab (MathWorks, Inc.). The Plexiglas^{TM} wings were immersed in a 2 m^3 (1 m×1 m×2 m) tank of mineral oil (density=0.88×10^3 kg m^{-3}; kinematic viscosity=115 cSt) and flapped at a Reynolds number of approximately 134. The wings had an aspect ratio of approximately 1.9 and were shaped like a wing of the fruit fly *Drosophila melanogaster* Meigen.

Kinematics

Wing kinematics among flying insects or between various types of flight manoeuvres mostly differ in more than one kinematic parameter, such as in stroke amplitude, angle of attack and rotational wing motion, which makes it difficult to assess the benefit of wing tip trajectory for vertical force production during clap-and-fling wing beat. We thus limited our experimental approach to generic patterns and tested the significance of stroke trajectory for clap-and-fling total force and vertical force augmentation by comparing 17 kinematic patterns with identical stroke amplitude, stroke frequency and *geometric* angle of attack with respect the horizontal, but different heaving motion (Fig. 2). Due to the various types of heaving motion, however, the *effective* angle of attack slightly varied between the tested kinematic patterns. Although none of the patterns used in this study exactly matched any of those found in flying insects, the various wing trajectories covered various categories of stroke shapes used by flying insects, such as oval or figure-eight shapes (Brodsky, 1994). The prescribed kinematic patterns were constructed using custom software routines (Matlab) in which various aspects of wing motion could be modified.

All experiments were conducted using a horizontal stroke plane, 160° stroke amplitude, 0.17 Hz stroke frequency and 50° angle of attack with respect to the horizontal. This angle of attack was slightly higher than the one used in a previous study (40°) and was chosen to avoid negative angles of incidence at some kinematic patterns (Dickinson et al., 1999) (Fig. 2C,F,G,O–Q). In all cases, we modelled a symmetrical stroke with similar velocity profiles in both half strokes (up-to-down ratio=1.0). Translational wing velocity was constant throughout the stroke cycle with accelerations only at the beginning and the end of each half stroke. Wing rotation was symmetric about stroke reversal, with 4% of the wing rotation occurring before and 4% after stroke reversal. A symmetrical wing rotation has commonly been found in most freely and tethered flying insects examined so far (e.g. Ellington, 1984a; Zanker, 1990a). All kinematic patterns were slightly smoothed to avoid sudden accelerations of the experimental apparatus. We produced various categories of kinematic patterns by systematically changing heaving motion during wing translation using a sinusoidal velocity profile with a peak-to-peak amplitude of 38° (Eqn 1, Fig. 2). During up- and downstrokes, the heaving angle was either in-phase or antiphase with respect to the translational part of the stroke and the heaving frequency was either equal to (0.17 Hz) or twice (0.35 Hz) the flapping frequency, respectively. For each half stroke, heaving angle can thus be expressed as:

$$\delta(\hat{t}) = 19^\circ \cdot a \cdot \sin(2 \cdot \pi \cdot \hat{t} \cdot b) , \quad (1)$$

where $\hat{t}$ is fraction of stroke cycle (0–1, beginning with downstroke), the variable a is either 1 (in-phase) or –1 (antiphase motion), the variable b is either 1 (0.17 Hz) or 2 (0.35 Hz, see above), and δ is heaving angle with respect to the horizontal (positive value means elevation). The equation produced 16 possible categories of stroke shapes and we included one further kinematic pattern in which the amplitude of the heaving angle was set to zero (pattern I, Fig. 2).

Due to the alignment of the wing hinges and the rigidity of the robotic wings, the generic kinematic patterns we used did not allow a full clap in which both wings physically touch along their entire surface (Lehmann et al., 2005). Due to this

limitation, the wings were not exactly parallel during the clap, and the wing bases were farther apart than the wing tips. Since previous research has shown that larger separation angles between the wings produce smaller magnitudes in vertical force augmentation, we adjusted the mean stroke angle for translation for the kinematic patterns to minimize the gap between the wings during the clap without permitting the wings to physically touch each other.

Force coefficients and pitching moment

In previous studies mean lift and drag coefficients for wing motion were derived from mean lift and drag averaged throughout the entire stroke cycle using a modified expression of equation 12 in Ellington (Ellington, 1984b; Lehmann and Dickinson, 1998). This equation, however, was developed for hovering flying insects beating their wings in a flat, horizontal stroke plane and may not account for changes in wing velocity due to heaving motion. Depending on the vector sum between horizontal and vertical velocity components, instantaneous wing velocity may differ from estimates based on horizontal velocity components only. We thus replaced Ellington's expression term for mean square of dimensionless angular wing velocity in the horizontal, by a term $\overline{\hat{\psi}^2}$, that takes into account both horizontal *and* vertical angular velocity. The modified expression can be written as:

$$\overline{C_{F(V)}} = 8 \cdot \overline{F_v} / \rho \cdot \Phi^2 \cdot n^2 \cdot R^2 \cdot S \cdot \overline{\hat{\psi}^2} \cdot \hat{r}_2^2(S) \, . \qquad (2)$$

In the equation above, $\overline{F_v}$ is the vertical weight-supporting force of a single wing averaged throughout the stroke cycle i.e. opposite to gravity, ρ is the density of the mineral oil, Φ is stroke amplitude defined as the angle that the wings cover during wing translation when projected into the horizontal plane, n is stroke frequency, R is wing length, S is total wing area, and $\hat{r}_2^2(S)$ is the squared non-dimensional radius of the second moment of wing area that characterizes wing shape [for nomenclature see Ellington (Ellington, 1984c)] (Fig. 3). Horizontal force coefficient was calculated by replacing vertical by horizontal force in the above equation. The mean square of non-

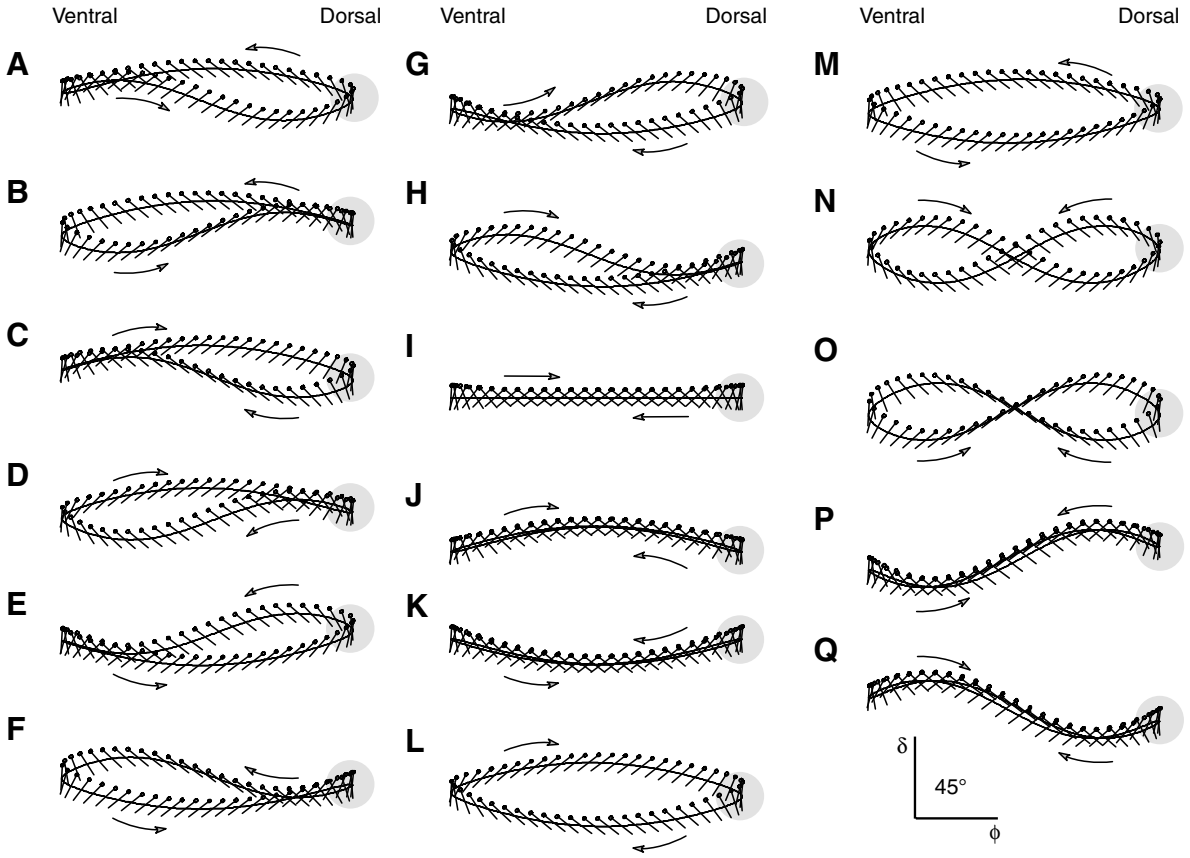

Fig. 2. (A–Q) Multiple categories of stroke patterns as used in the present study. The black line shows the tip trajectory of the moving wing with the position of superimposed chordwise wing segments every 0.125 s. Arrows indicate the direction of wing motion during up- and downstroke. The small circle at each wing segment indicates the leading edge. In all experiments the angle of attack of the beating wing with respect to the horizontal was kept constant at 50° while the vertical elevation of the wing trajectory (heaving motion) from the horizontal stroke plane systematically varied within the up- and downstroke. Stroke amplitude (160°), cycling frequency (0.17 Hz), start (–4% stroke cycle) and end (4% stroke cycle) of wing rotation and up- to downstroke ratio (0.5) are the same in all figures. Wing separation angle at ventral excursion is approximately 40°. Grey area indicates the time during dorsal stroke reversal at which left and right wing perform clap-and-fling without physically touching each other.

dimensional angular wing velocity, $\overline{\hat{\psi}^2}$, is equal to the temporal integral of the vector sums of flapping and heaving angular velocities and depends on heaving motion as follows:

$$\overline{\hat{\psi}^2} = \int_{\hat{t}=0}^{1}\{\cos^2\delta(\hat{t})\cdot[\mathrm{d}\hat{\phi}(\hat{t})/\mathrm{d}\hat{t}]^2 + (\delta_{max}-\delta_{min})^2\cdot\Phi^{-2}\cdot[\mathrm{d}\hat{\delta}(\hat{t})/\mathrm{d}\hat{t}]^2\}\cdot\mathrm{d}\hat{t}\,. \quad (3)$$

In this equation, the variables $\hat{\phi}$ and $\hat{\delta}$ are instantaneous normalized stroke and heaving angles ranging from –1 to 1, respectively, and δ_{max} and δ_{min} are maximum and minimum heaving angles of 19° and –19°, respectively. The constant factor, $(\delta_{max}-\delta_{min})/\Phi$, on the right hand side of the sum adjusts heaving velocity according to the amplitude ratio between flapping and heaving angle. Following Ellington's nomenclature for normalized stroke angles (Ellington, 1984a),

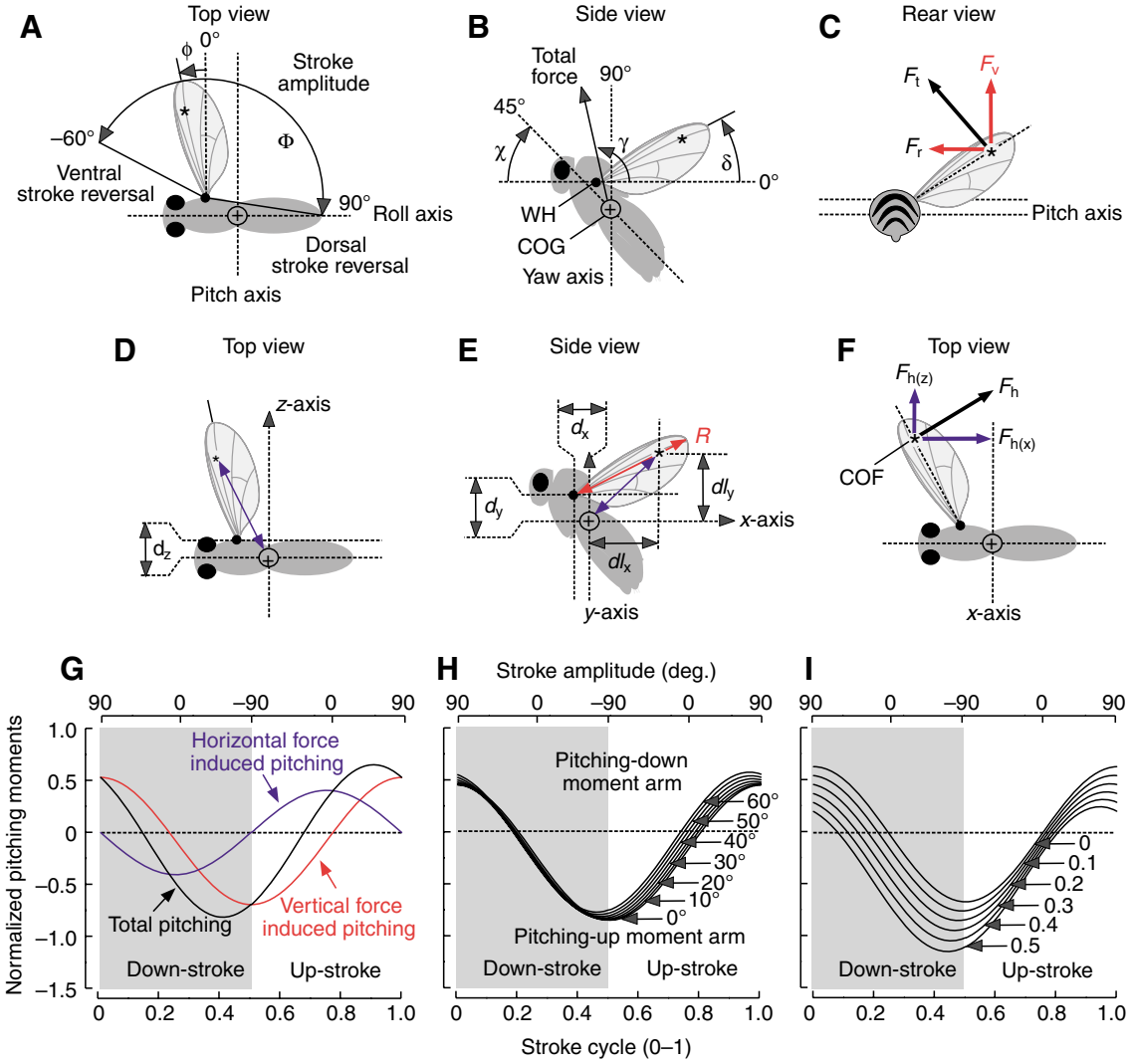

Fig. 3. Rotational axes, angles, and length of relative moment arms for pitching within the stroke cycle. (A) Instantaneous stroke angle ϕ, stroke amplitude Φ; (B) body angle χ, heaving angle δ during wing translation and inclination of total force vector γ. (C) Lift normal to the wing surface (black) is the vector sum between vertical force F_v and a radial force component F_r. See text for more details. (D–E) Location of the animal's centre of mass in the z-plane and length of moment arm for pitching moments in the horizontal dl_x and vertical direction dl_y. (F) Horizontal force of the flapping wing is the vector sum of a horizontal component $F_{h(x)}$ and a force component $F_{h(z)}$ in z-direction. COF, centre of force producion. (G) Simplified hypothetical alteration in length of the moment arm for each angular position of the longitudinal wing axis within a horizontal stroke plane and without heaving motion. Total pitching moments (black) are the sum of moments produced by vertical force F_v (red) and horizontal force $F_{h(x)}$ (blue). Moments were calculated using Eqn 13 and Eqn 14 and plotted for a complete stroke cycle with 180° stroke amplitude. In the example shown body angle is 30°, normalized distance $\hat{d}$ between wing hinge and COG is 0.2 wing length, and wing length R, horizontal $F_{h(x)}$ and vertical force F_v are 1.0, respectively. (H) Examples of changes in length of moment arm for pitching plotted at various body angles (χ=0–60°, R=1, $F_{h(x)}$=1, F_v=1, $\hat{d}$=0.2, δ=0°). (I) Examples of alterations in length of moment arm for pitching at various distances $\hat{d}$ between wing hinge and COG ($\hat{d}$=0–0.5, R=1, $F_{h(x)}$=1, F_v=1, χ=30°). Positive and negative arm for pitching moments produce pitching down and up moments, respectively. *Point of attack for mean force vector acting on the wing at 0.65 wing length; circled cross, centre of body mass (COG) and filled circle, wing hinge (WH) of the virtual insect.

we expressed both angles in the above equation using the following two equations:

$$\hat{\phi}(\hat{t}) = 2\cdot[\phi(t)-\bar{\phi}] / \Phi \quad (4)$$

and

$$\hat{\delta}(\hat{t}) = 2\cdot[\delta(t)-\bar{\delta}] / (\delta_{max}-\delta_{min}) , \quad (5)$$

in which $\bar{\phi}$ and $\bar{\delta}$ are mean stroke and heaving angle, respectively. For kinematic patterns exhibiting sinusoidal heaving motion during up and downstroke of 0.17 (Fig. 2J–M) and 0.35 Hz (Fig. 3N–Q), the variable $\hat{\psi}^2$ amounts to 16.3 and 19.6, respectively. Pattern in which heaving frequency was different in both halfstrokes $\hat{\psi}^2$ is 18.0 (Fig. 2A–H), whereas in a horizontal stroke without heaving motion $\hat{\psi}^2$ is 16.0 (Fig. 2I). Besides the modifications in wing velocity, heaving motion within a stroke cycle also changes the estimation of mean lift coefficient since this measure depends on the vertical aerodynamic force component that counterbalances the animal's mass (F_v, Fig. 3C). Due to the angular displacement of the wing from the horizontal, the vector F_v is no longer normal to the direction of wing motion or the direction of the oncoming air, nor in line with the net thrust vector. Wings flapping with positive or negative heaving angles thus produce a radial force component towards or away from the insect body (F_r, Fig. 3). However, even at maximum heaving angle of 19°, this force vector is still relatively small and only amounts to 5% (cosine 19°) of lift produced normal to the wing surface (black, Fig. 3C). Insect wings that beat in a horizontal plane thus potentially produce higher lift coefficients because in this case the radial force component F_r is zero and all lift produced within the stroke cycle may help to support the animal's weight. Thus, throughout the manuscript we replaced the terms lift and drag by 'vertical force' and 'horizontal force', respectively, that approximate lift and drag during near-horizontal wing motions (Fig. 3C,F).

Since the contribution of clap-and-fling to vertical force production and the control of rotational moments around the body axes depend on wing tip trajectory, clap-and-fling effect may change during steering behaviour. In a two-winged insect, symmetric changes in roll and yaw moments of both wings may be of minor importance for steering control, because these effects may cancel each other out due to the mirror-symmetry of the two flapping wings. By contrast, the situation for pitch is different because in a left–right symmetrical stroke pattern, both wings contribute collectively to the changes in pitching moment. For the above reasons, we disregarded roll and yaw in this study, and solely estimated the pitching moments acting on an imaginary body of the robotic wing. These measures were derived from vertical and horizontal forces of a single wing by approximation of the moment arm between the centre of force production, COF, and the fly's centre of mass, COG (Fig. 3). We thereby assumed that at all times the COF is located on the longitudinal wing axis and at 0.65 wing length, regardless of the underlying aerodynamic mechanisms employed for force production (Birch and Dickinson, 2001; Ramamurti and Sandberg, 2001). Due to the lack of experimental data on radial forces acting parallel to the wing's longitudinal axis such as centrifugal forces, we ignored this force component for the production of pitching moments. Instantaneous moments produced by a single wing around the imaginary pitch axis of the mechanical insect, T_P, may be written as:

$$T_P(\hat{t}) = F_v(\hat{t})\cdot dl_x(\hat{t}) + F_{h,x}(\hat{t})\cdot dl_y(\hat{t}) , \quad (6),$$

where $F_v(\hat{t})$ and $F_{h,x}(\hat{t})$ are instantaneous vertical and horizontal forces normal to the pitching axis, respectively, whereas dl_x and dl_y are the horizontal and vertical distances (moment arms) between COF and COG (d_x, d_y, d_z). The vertical, d_y, and horizontal distances, d_x, between the wing hinge and the centre of body mass depend on the distance, d, between wing hinge and the centre of body mass, and body angle, χ, with respect to the horizontal (Fig. 3B). We expressed the horizontal distances dx and dy by the following equations:

$$d_x = \cos\chi\cdot d , \quad (7)$$

and

$$d_y = \sin\chi\cdot d , \quad (8)$$

respectively. The vertical moment arm dl_x changes with both stroke angle from approximately 90° at the dorsal to approximately to –70° during the ventral excursion of the wing and heaving angle, but also depends on the distance between the wing hinge and the fly's COG (Fig. 2, Fig. 3A,B). The horizontal moment arm for pitching can thus be written as:

$$dl_x = 0.65R\cdot\sin(\phi)\cdot\cos(\delta) - d_x . \quad (9)$$

In contrast to the horizontal moment arm for vertical force, the vertical moment arm, dl_y, for horizontal force is independent of stroke angle and only depends on the wing's heaving motion. We expressed the vertical moment arm by the following relationship:

$$dl_y = 0.65R\cdot\sin(\delta) + d_y . \quad (10)$$

The latter equation suggests that in insects in which the horizontal stroke plane runs through the COG, horizontal forces may not induce pitching moments because the moment arm is zero.

In an aerodynamic framework, drag and thus horizontal force F_h is always positive during both up- and downstroke. When we consider pitching moments, however, F_h during the downstroke may consistently produce negative 'nose-up' pitching moments, whereas during the upstroke F_h produces positive 'nose-down' moments. We modelled this behaviour by introducing a simple rectifying step function $K(\hat{t})$ that is negative during downstroke and positive during upstroke:

$$K(\hat{t}) = -1, \text{ for } 0 \leqslant \hat{t} < 0.5, \text{ and } K(\hat{t}) = 1, \text{ for } 0.5 \leqslant \hat{t} < 1.0 . \quad (11)$$

Besides the sign of the horizontal force during up- and downstroke, F_h may not produce pitching moments at stroke angles of 90° (dorsal wing reversal) and –90° (ventral reversal), because in this case F_h is acting parallel to the pitching axis (x-axis, Fig. 3F). Thus, the effective horizontal component for

pitching, $F_{h(x)}$, depends on stroke angle and should thus be derived from horizontal force as follows:

$$F_{h(x)}(t) = F_h(t)\cdot\cos\phi \ . \quad (12)$$

Combining all equations mentioned, the instantaneous pitching moment produced by instantaneous vertical, $T_{P,F(V)}(t)$, and horizontal force, $T_{P,F(H)}(t)$, within a stroke cycle may be derived from the following expressions:

$$T_{P,F(V)}(t) = R\cdot F_v(t)\cdot[0.65\cdot\sin\phi(t)\cdot\cos\delta(t) - \cos\chi\cdot\hat{d}] \ , \quad (13)$$

and

$$T_{P,F(H)}(t) = R\cdot K(t)\cdot F_{h(x)}(t)\cdot[0.65\cdot\sin\delta(t) + \sin\chi\cdot\hat{d}] \ , \quad (14)$$

where total instantaneous pitching moment is the sum of both equations. In the latter equations, we used Ellington's form of dimensionless distance, $\hat{d}$, that may be derived from wing length by:

$$\hat{d} = d\cdot R^{-1} \ . \quad (15)$$

Our simple model suggests that pitching moments are independent of thoracic width and thus the distance d_z in Fig. 3D, whereas d_z should be considered for estimations of yaw and roll moments. Fig. 3G shows how the moment arms for vertical and horizontal force-induced moments potentially alter pitching moments, assuming constant force production throughout a complete stroke cycle (Eqn 13 and Eqn 14). In this calculation, two variables were set equal to measures found in the fruit fly that are (i) 66° for body angle during hovering condition (Götz, 1983) and (ii) a value of 0.2 for the relative distance between wing hinge and COG (Lehmann, 1994), whereas heaving angle was 20°, and the remaining parameters (R, F_v, F_h) were set to 1.0. The theoretical framework, moreover, predicts relatively small changes in total pitching arm when changing body angle from 0° and 60° in a horizontal stroke plane as found in some hovering insects (R=1, F_v=1, F_h=1, δ=0°, Fig. 3H). By contrast, changes in distance between wing hinge and COG apparently alter pitching moments more strongly by increasing nose-up moments with increasing distance between both geometric measures (R=1, F_v=1, F_h=1, χ=30°, Fig. 3I). Since the body angle decreases considerably during forward flight of the fruit fly, we used the following mean constants for deriving pitching moments on the virtual body of our robotic wing: R=25 cm, $\hat{d}$=0.2, and χ=30° for all kinematic patterns and throughout the entire manuscript, if not stated otherwise, whereas the remaining values were derived from both the kinematics and the force measurements of the robotic model (David, 1978).

Experimental procedure and statistical analysis

We derived lift augmentation due to clap-and-fling from the difference of mean lift measured at two experimental conditions: (i) flapping the ipsilateral wing and (ii) flapping the ipsi- and a contralateral mirror wing in close distance. The differences between both measurements were either expressed in units of force or normalized to the performance of a single wing and expressed as percentage change. Alterations of pitching moments due to clap-and-fling on the virtual fly body were calculated accordingly. Throughout the manuscript data are given as means ± standard deviation (s.d.).

Results

Force coefficients

The wing beat patterns in Fig. 2 generated pronounced changes in total vertical force production during the clap-and-fling manoeuvre of the robotic wings. Among the 17 stroke patterns, values of mean total force, i.e. the vector sum of

Table 1. *Mean forces and mean force coefficients during motion of a single wing and clap-and-fling force augmentation for 17 stroke patterns*

	Pattern																
	A	B	C	D	E	F	G	H	I	J	K	L	M	N	O	P	Q
$\overline{F}$ (mN)	542	519	499	500	511	519	509	510	539	509	517	497	519	524	511	508	522
$\overline{F_h}$ (mN)	436	438	429	405	420	442	438	422	444	422	437	418	428	413	454	422	440
$\overline{F_v}$ (mN)	322	279	256	292	292	271	260	285	305	285	277	269	293	323	234	282	281
$\overline{C_F}$	2.85	2.73	2.62	2.62	2.68	2.72	2.67	2.68	3.03	2.75	2.79	2.62	2.74	2.43	2.36	2.49	2.56
$\overline{C_{F(H)}}$	2.04	2.05	2.00	1.90	1.96	2.07	2.05	2.22	2.50	2.24	2.32	2.16	2.22	1.56	1.71	1.69	1.76
$\overline{C_{F(V)}}$	1.51	1.31	1.19	1.36	1.36	1.27	1.21	1.34	1.72	1.51	1.46	1.40	1.52	1.22	0.88	1.12	1.12
$\overline{A_F}$ (mN)	41	28	54	34	29	49	50	36	38	40	51	56	34	20	71	32	44
$\overline{A_{F(H)}}$ (mN)	37	25	41	24	27	39	38	30	32	30	41	42	33	21	54	28	34
$\overline{A_{F(V)}}$ (mN)	20	13	37	24	11	30	34	20	21	27	30	37	13	5	49	17	28
$\overline{A_F}$ (%)	7.1	5.1	9.7	6.3	5.3	8.6	9.0	6.6	6.6	7.30	8.9	10.1	6.2	3.6	12.2	6.0	7.8
$\overline{A_{F(H)}}$ (%)	7.8	5.3	8.6	5.6	6.1	8.1	8.1	6.7	6.7	6.6	8.6	9.2	7.1	4.9	10.6	6.2	7.2
$\overline{A_{F(V)}}$ (%)	5.8	4.5	12.5	7.6	3.5	9.9	11.5	6.4	6.4	8.7	9.7	12.1	4.2	1.4	17.4	5.6	9.2

Absolute augmentation of mean normal flight force, $\overline{A_F}$, and mean vertical force, $\overline{A_{F(V)}}$, are calculated from the difference between forces produced by two wings and one wing flapping. $\overline{C_F}$, mean force coefficient of normal flight force of a single flapping wing; $\overline{C_{F(V)}}$, mean vertical force coefficient of a single flapping wing. All relative augmentation values are given in percent change normalized to single wing performance.

Patterns A–Q correspond to the kinematic patterns shown in Fig. 2.

vertical and horizontal force, and mean vertical force averaged throughout the stroke, were scattered around 0.55±0.01 N and 0.28±0.02 N (N=17 patterns), respectively. Mean normal force coefficient and mean vertical force coefficient amounted to 2.67±0.16 and 1.32±0.20 (N=17 patterns), respectively (Table 1). Pattern I, in which the wing moves in the horizontal without heaving motion produced the largest vertical force coefficient of approximately 1.72 (Fig. 2), whereas figure-eight stroke pattern O showed the smallest vertical force coefficient of 0.88, among all tested kinematics (Table 1). Mean horizontal force coefficients covaried significantly with mean vertical force coefficients among the tested patterns and more than 66% of the variance in horizontal force coefficient can be explained by the changes in vertical force coefficient (linear regression fit, $\overline{C_{F(H)}}=0.68+1.01\overline{C_{F(V)}}$, $R^2=0.66$, $P<0.0001$).

Force augmentation

In all tested cases, clap-and-fling effects reinforced both total force acting approximately normal to the wing surface by 3.6–12.2% ($\overline{A_F}$, Table 1) and vertical force production by 1.4–17.4% ($\overline{A_{F(V)}}$, Table 1). The smallest values of total force F and vertical force F_v augmentation of 3.6% and 1.4%, respectively, were found in a figure-eight wing kinematics in which the angle of attack during mid down- and upstroke is relatively large due to the decreasing and increasing heaving angle, respectively (Fig. 2N). By contrast, a mirrored figure-eight kinematics in which the geometric angle of attack with respect to the direction of wing motion is small during mid up- and mid downstroke produced maximum total force and vertical force augmentation of approximately 12.2% and 17.4%, respectively (Fig. 2O). The latter extremes suggest that the pronounced vertical force enhancement of pattern O might be attributable to the low overall performance of this kinematic pattern ($\overline{C_{F(V)}}=0.88$, Fig. 2) compared to the elevated performance produced by pattern N ($\overline{C_{F(V)}}=1.22$, Fig. 2). Fig. 4 shows this relationship, demonstrating that vertical force augmentation due to dorsal wing–wing interaction significantly decreases with increasing mean vertical force production (Fig. 4A) whereas vertical force augmentation is independent from vertical force coefficient (Fig. 4B, Table 2). Interestingly, the regression analysis on all 17 kinematic patterns revealed that mean force augmentation is independent of total force produced by a single wing (P=0.13, Table 2) whereas mean horizontal force augmentation due to clap-and-fling increases significantly with increasing mean horizontal force produced throughout the entire stroke cycle (P=0.02, Table 2).

A previous study on dorsal wing–wing interaction in robotic wings showed that force- and lift augmentation depend on several factors, including the speed of wing rotation during stroke reversal (Lehmann et al., 2005). Although the dependency between lift augmentation and rotational speed appears to be complex, lift augmentation due to clap-and-fling largely increases with decreasing rotational speed and thus with increasing duration of wing rotation at the stroke reversals. To further examine the dependencies between lift augmentation and rotational wing motion, we calculated the force contribution by wing rotation (the sum of rotational circulation and wake capture) using a conventional quasi-steady model for force production, identical to a procedure published previously (Dickinson et al., 1999). The difference between the quasi-steady force estimate and measured force, is termed 'rotational effect' throughout the manuscript. Fig. 4C shows that rotational effect apparently differs between the tested kinematic patterns and enhances vertical force by up to 25% (131 mN, pattern O) or attenuates vertical force by up to –10% (–52 mN, pattern H) of total vertical force production. Linear regression analysis suggests that clap-and-fling enhanced vertical force augmentation is independent from

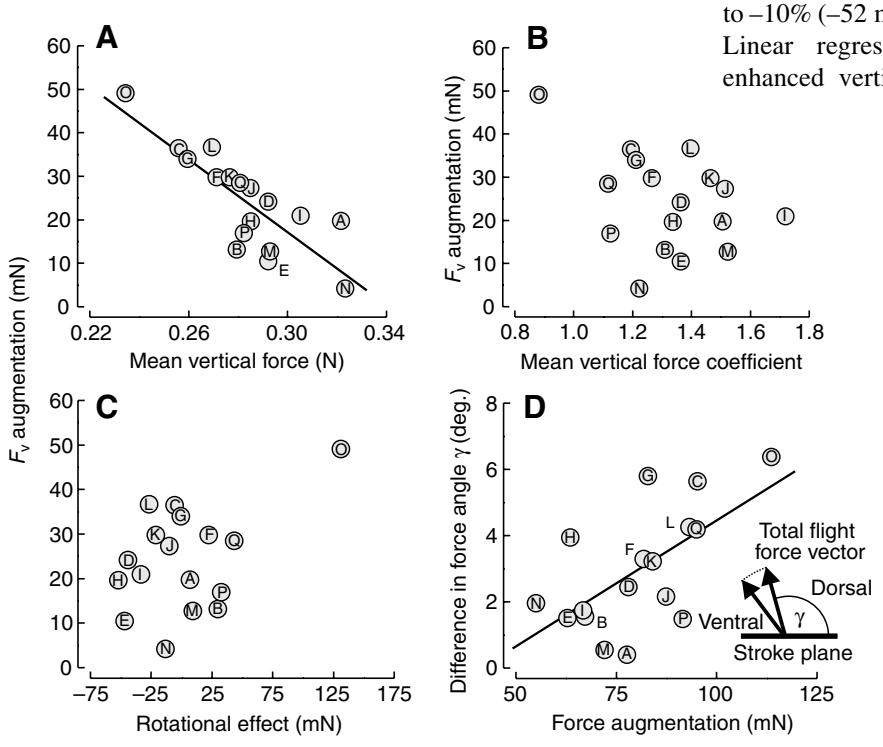

Fig. 4. Vertical force augmentation due to dorsal wing–wing interaction in 17 gross kinematic patterns. (A) Augmentation of vertical force (two-wing minus one-wing performance) plotted as a function of mean vertical force produced throughout the stroke cycle, (B) vertical force augmentation plotted against mean vertical force coefficient based on a conventional quasi-steady approach, (C) vertical force augmentation plotted against the relative contribution of wing rotation (rotational effect) and wake capture to quasi-steady translational vertical force, and (D) change in orientation of total force vector (pictogram) due to dorsal clap-and-fling wing–wing interaction. Letters plotted on or close to data points correspond to the letters of the kinematic patterns shown in Fig. 2.

Table 2. *Parameters of linear regression fits between aerodynamic measures and various kinematics patterns*

Dependencies (y) *vs* (x)	*y*-intercept	Slope	R^2	*P*	Fig.
$\overline{A_F}$ (mN) *vs* $\overline{F}$ (N)	317±148	–459±288	0.15	0.13^{NS}	–
$\overline{A_{F(H)}}$ (mN) *vs* $\overline{F_h}$ (N)	–131±68.2	403±159	0.30	0.02*	–
$\overline{A_{F(V)}}$ (mN) *vs* $\overline{F_v}$ (N)	142±21.5	–418±75.8	0.67	<0.001***	4A
$\overline{A_{F(V)}}$ (mN) *vs* $\overline{C_{F(V)}}$ (N)	54.5±18.3	–22.8±13.7	0.16	0.12^{NS}	4B
$\overline{A_F}$ (mN) *vs* $\overline{F_{rot}}$ (mN)	80.2±2.83	0.22±0.07	0.43	0.004**	–
$\overline{A_{F(H)}}$ (mN) *vs* $\overline{F_{rot}}$ (mN)	41.9±2.00	0.11±0.05	0.28	0.03*	–
$\overline{A_{F(V)}}$ (mN) *vs* $\overline{F_{rot}}$ (mN)	24.2±2.55	0.12±0.06	0.20	0.07^{NS}	4C
$\overline{A_\gamma}$ (deg.) *vs* $\overline{A_F}$ (mN)	–3.15±2.00	0.08±0.03	0.39	0.008**	4D
$\overline{A_\gamma}$ (deg.) *vs* $\overline{A_{F(V)}}$ (mN)	–0.25±0.63	0.13±0.02	0.68	<0.0001***	–
T_P (Nmm) *vs* $\overline{F_v}$ (N)	15.8±28.9	–77.6±102	0.04	0.46^{NS}	8A
$\overline{A_{T(P)}}$ (Nmm) *vs* $\overline{F_v}$ (N)	14.6±2.94	–47.1±10.4	0.58	<0.001***	8C
$\overline{A_{T(P)}}$ (Nmm) *vs* $\overline{A_{F(V)}}$ (mN)	–1.01±0.53	0.09±0.02	0.60	<0.001***	8D

Forces and force coefficients are mean values averaged throughout a stroke cycle for a single flapping wing. *N*=17 kinematic patterns.

Asterisks indicate mean significance level of slope: *P<0.05, **P<0.01, ***P<0.001. NS, not significant. For further abbreviations see List of symbols and abbreviations.

rotational effect (linear regression fit slope, P=0.07, Table 2), whereas total force and horizontal force augmentations increase significantly with increasing rotational force (P=0.004 and P=0.03, respectively, Table 2). This finding contradicts the hypothesis that force augmentation in general should be independent of rotational effects among the tested kinematic patterns, because these are similar in rotational rate and timing at the stroke reversals. Consequently, the relationship between force augmentation due to clap-and-fling and force augmentation due to rotational effects is not solely attributable to the translational variation of the kinematic patterns that predominates force production. A further prominent finding of clap-and-fling wing beat is the change in total flight force angle with respect to the horizontal. Due to the increase in force production when both wings interact, the force vector tilts slightly forward up to 6.4° in figure-eight pattern O, significantly increasing with a slope of 0.08 and 0.13° mN^{-1} with increasing force and vertical force augmentation, respectively (Fig. 4D, Table 2).

Temporal distribution of lift augmentation

The above data show that vertical force augmentation due to clap-and-fling apparently depends on vertical force production (Fig. 4A) but not on vertical force coefficient (Fig. 4B). Thus, vertical force augmentation may be different in stroke patterns exhibiting approximately the same vertical force coefficient. For example, the pear-shaped stroke pattern A, the pattern J and the oval pattern M (Fig. 2) all produce a vertical force coefficient near 1.51 (Table 1), but vary in their ability to enhance vertical force when the robotic wing performs a clap-and-fling wing beat ($\overline{A_{F(V)}}$=20 mN in A; 27 mN in J and 13 mN in M). Moreover, the time traces in Fig. 5 show that the temporal distribution of forces throughout the entire stroke cycle slightly vary between the three exemplary kinematic patterns. A characteristic feature in all vertical and horizontal force traces is the pronounced increase of force during the fling part, compared to a single flapping wing. However, a detailed comparison between one- and two-wing flapping conditions revealed that the forces change throughout the stroke cycle in a more complex manner.

To highlight the temporal distribution of lift enhancement when flapping both wings, we plotted the differences between one- and two-wing flapping conditions for the three stroke patterns A, J and M in Fig. 6A–C. The data show quite complex changes in vertical force due to dorsal wing–wing interaction with temporal characteristics similar to force traces published previously for the stroke pattern of the fruit fly *Drosophila* (Lehmann et al., 2005). In the latter study, clap-and-fling mediated lift enhancement was broken down into six distinct positive and negative force peaks scattered in time over the entire wing beat cycle. The averaged data in Fig. 6D (*N*=17 kinematic patterns) show similar major peaks, as indicated by the letters I–VI: (i) a comparatively long-lasting but weak attenuation of vertical force during the late upstroke (peak I), (ii) a small abrupt decrease of vertical force immediately after the clap (peak II), (iii) a sharp, large peak during the fling motion of the wings (peak III), (iv) a small biphasic change in vertical force production (peaks IV and V) after the wings had separated and continued the downstroke, and (v) a small positive peak (peak VI) at the beginning of the upstroke. Moreover, Fig. 6D shows that the standard deviation around peak I is relatively small, suggesting that upstroke vertical force attenuation is a common feature of wing-wing interaction in all 17 tested kinematic patterns. Although the complex distribution of vertical force enhancement and attenuation over time is of minor importance for the ability of an insect to overcome gravity, it determines rotational moments around the roll, pitch and yaw axes of the insect body due to the changing moment arms, and thus the animal's ability to control body posture during manoeuvring flight.

Pitching moment during wing–wing interaction

We calculated the temporal distribution of the pitching moments on the imaginary body of our mechanical 'insect',

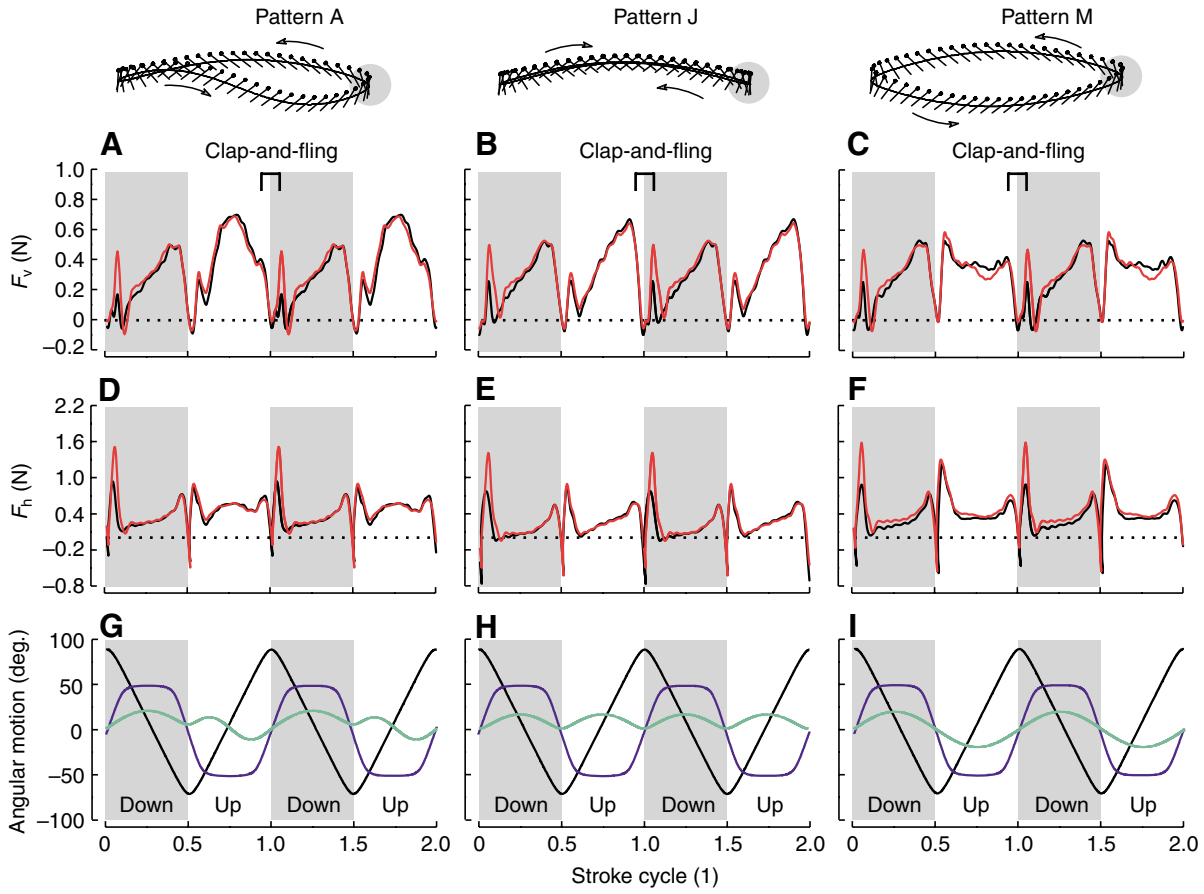

Fig. 5. Forces generated by three different kinematic patterns that yield approximately the same mean vertical force coefficients (~1.51) during wing flapping. Stroke pattern in the left, middle and right column is A, J and M, respectively (Fig. 2). (A–C) Vertical force F_v and (D–F) horizontal force F_h acting on the wing for one wing flapping (black) and while flapping a mirror wing in close distance on the other side of the robotic flapper (red). (G–I) Translational angular wing motion (black), the wing's angle of attack (blue) and heaving motion (green) of two stroke cycles for the three kinematic patterns A, J, M.

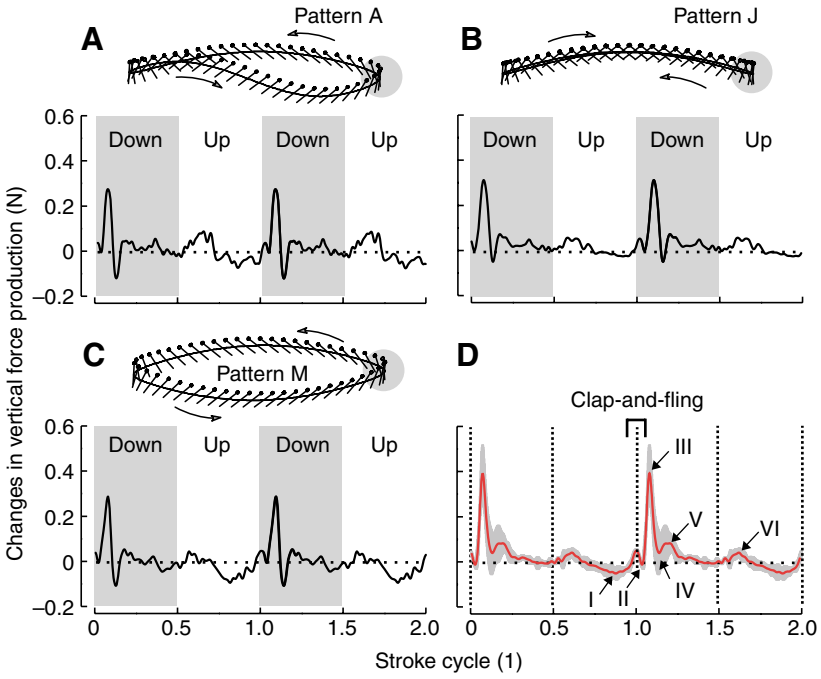

Fig. 6. (A–C) Temporal distribution of vertical force augmentation for three kinematic patterns and (D) mean vertical force augmentation during clap-and-fling wing beat. Data are plotted as the difference (2–1) between the performance of one (1) and two (2) flapping wings. (A–C) Kinematic patterns (pictograms) produced the same mean vertical force coefficient during wing motion (~1.51). (D) Mean values (red) ± s.d. (grey) of all 17 kinematic patterns. Force peaks are labelled according to Lehmann et al. (Lehmann et al., 2005).

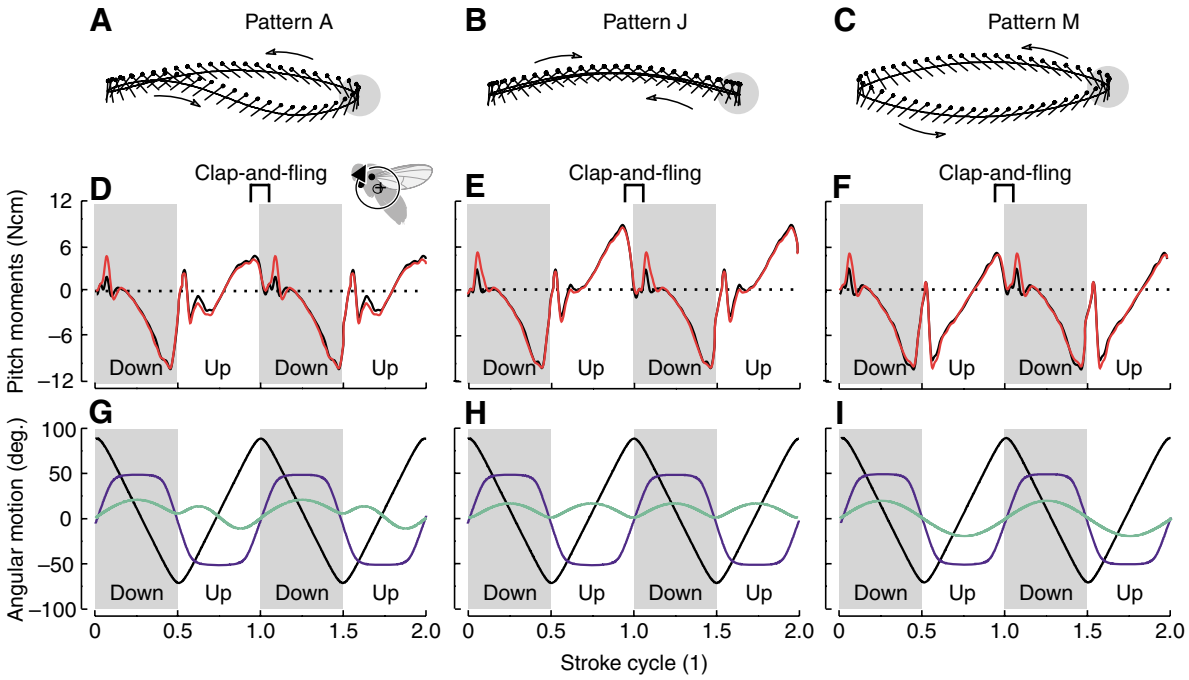

Fig. 7. (A–I) Kinematics and moments around the imaginary pitch axis of the electromechanical flapper produced at three experimental conditions. (A–C) Pictograms above each column indicate the kinematic patterns used for comparison (mean vertical force coefficient in all patterns is ~1.51). (G–I) Translational angular wing motion (black), the wing's angle of attack (blue) and heaving motion (green) of a single stroke cycle for the three kinematic patterns A,J,M. Black=single wing performance; red=performance when flapping two wings; body angle χ=30° and distance $\hat{d}$=0.2 wing length.

employing a simplified analytical model (cf. Materials and methods). Fig. 7 shows time traces for the three example stroke patterns A, J and M. Similar to the temporal distribution of vertical and horizontal force production within the stroke cycle, the data reveals a quite complex pattern for instantaneous pitching moments. The major results can be summarized as follows. (i) The mean pitching moments of all tested patterns are scattered around zero whereby only 5 of the 17 patterns produced positive nose-down moments (C,D,G,H,L) at 30° body angle and distance $\hat{d}$ of 0.2 wing length (Fig. 8A). Moreover, mean pitching moment is independent of total lift generated by a single wing (P=0.46, Table 2). (ii) Since the length of the moment arm for pitch is most favourable during ventral and dorsal stroke reversal, all tested kinematic patterns produced a strong nose-down pitching moment during the fling part of wing motion (Fig. 8B). At this point pitching moments vary strongly among the tested kinematic patterns (variance, Fig. 8B). (iii) Pitching moments due to clap-and-fling significantly decrease with increasing mean lift production (P<0.001, Table 2) whereas moments increase significantly with increasing mean lift augmentation (P<0.001, Fig. 8C,D, Table 2). Mean pitching augmentation due to clap-and-fling amounts to approximately 21% (1.27±1.37 Nmm) of pitching moments produced by a single wing (6.11±0.90 Nmm, Fig. 8D). (iv) Clap-and-fling induced pitching moments slightly depend on body angle (0–60°, Fig. 8E) but more strongly on the normalized distance between wing hinge and COG ranging from 0 to 0.9 wing length (Fig. 8F).

Fig. 8E suggests, moreover, that an insect might achieve similar clap-and-fling induced pitching moments even at different body angles. By contrast, increasing the distance between wing hinge and COG shortens the moment arm for pitching during the dorsal part of the stroke cycle, and the animal would experience an increase in negative nose-up pitching moments. The examples (pattern J and M) in Fig. 8F show that, under certain conditions, clap-and-fling induced pitching moments may even change algebraic sign with increasing distance $\hat{d}$. This finding matters in this respect, because the fruit fly actively contracts and deflects the abdomen during steering behavior (±100 μm) that likely leads to small relative changes in the position of COG (Zanker, 1988a; Zanker, 1988b). Thus, within the limits of the analytical model for rotational moments, our data suggest that the direction of pitching moments might depend on several locomotor actions including clap-and-fling wing beat and abdominal motion. The slope between $\hat{d}$ and augmentation of pitching moments slightly differs among the 17 tested patterns and ranges from -2.9×10^3 Nmm^{-1} (y–intercept=1.2×10^3 Nmm) in figure-eight pattern N to -12.7×10^3 Nmm^{-1} (y-intercept=6.2×10^3 Nmm) in figure-eight pattern O (three examples are shown in Fig. 8F).

Discussion

This study experimentally explored the significance of wing tip trajectory for the benefit of clap-and-fling wing beat in a 3D electromechanical insect wing. This device moved an ipsi- and

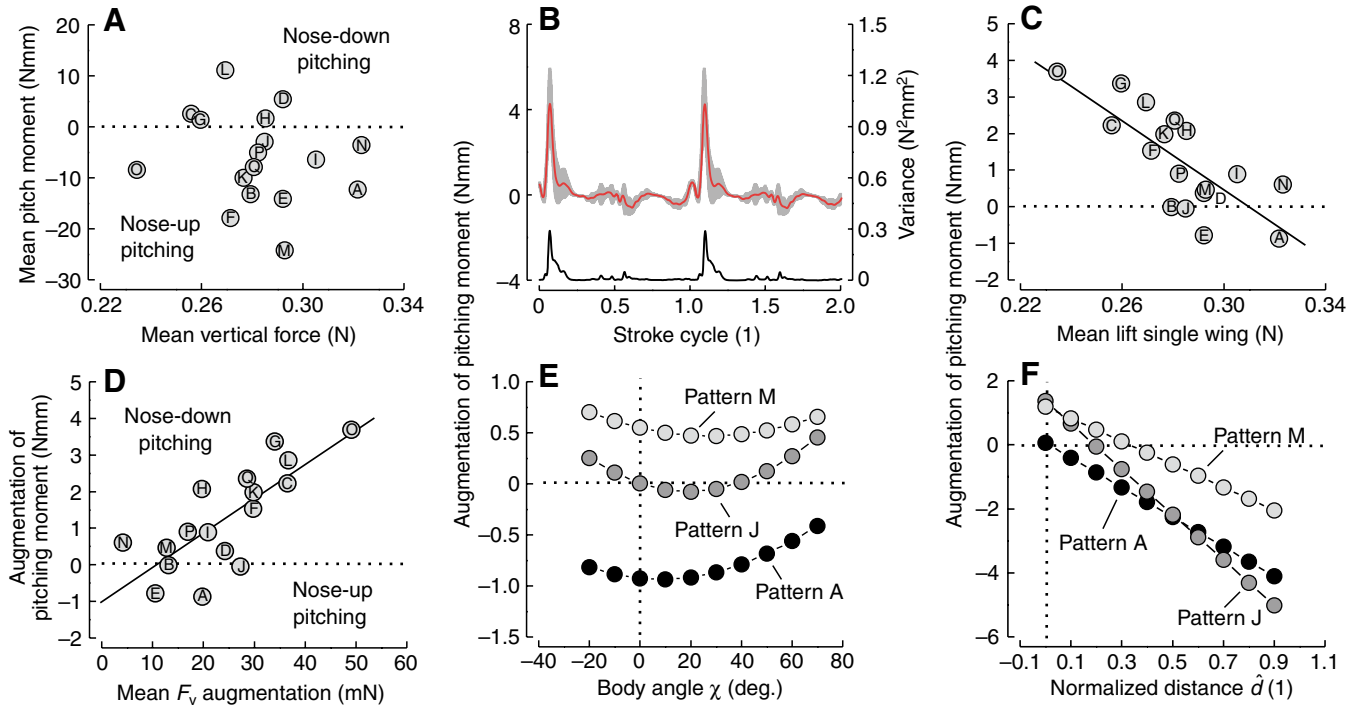

Fig. 8. Single wing and clap-and-fling induced pitching moments at various flapping conditions. (A) Mean pitching moment produced by a single wing, assuming a body angle of 30° and a distance between wing hinge and COG of 0.2 wing length. (B) Mean temporal distribution of pitching moment augmentation (red, left scale) ± s.d. (grey area) due to clap-and-fling wing beat of all 17 kinematic patterns used in the present study. Black line (right scale) indicates variation in the data set during two complete stroke cycles. (C,D) Augmentation of pitching moment due to clap-and-fling plotted against mean vertical force $\overline{F_v}$ in *C* and mean vertical force augmentation in *D*. (E,F) Alteration in pitching moment for the three kinematic examples in Figs 5–7, shown as a function of body angle χ at $\hat{d}$=0.2 wing length in *E* and as a function of distance $\hat{d}$ between wing hinge and COG at a body angle of 30° in *F*.

contralateral wing according to 17 pre-programmed kinematic patterns with different heaving motion (Fig. 2). The most important results may be summarized as follows. (i) Clap-and-fling induced total force augmentation appears to be independent of total mean force production of a single wing, whereas vertical force augmentation significantly decreases with increasing mean vertical force production (Fig. 4, Table 2). (ii) Vertical force augmentation is independent of rotational effect that is the sum of rotational circulation and wake capture. (iii) Vertical force augmentation may distinctly vary between stroke patterns, exhibiting approximately the same mean vertical force coefficient (Table 1). (iv) Among all tested kinematic patterns, most of the variation in vertical force augmentation within the stroke cycle occurs during fling (Fig. 6D). (iv) Mean pitching moments are independent of mean vertical force production of a single wing, whereas clap-and-fling induced pitching moments significantly co-vary with both mean vertical force coefficient and vertical force augmentation due to clap-and-fling. Pitching augmentation averaged among all tested kinematic patterns, amounts to approximately 21% of the mean pitching moments produced by single flapping wings. (v) Eventually, depending on body angle and the distance between wing hinge and the centre of body mass, augmentation of pitching moments vary distinctly and may produce both small nose-down and nose-up moments at similar kinematic patterns (Fig. 8E,F).

Changes in wing trajectory during steering behaviour

Many insects use clap-and-fling wing beat to boost lift performance or during flight manoeuvres (Cooter and Baker, 1977; Ellington, 1984a; Marden, 1987). Since the contribution of clap-and-fling to lift production and the control of rotational moments around the body axes depends on wing tip trajectory, clap-and-fling effect may change during steering behaviour. In general, kinematic variables such as wing path, stroke frequency, amplitude and angle of attack, including the underlying neuromuscular activity have been measured during tethered flight of several insect species such as *Drosophila* (Götz, 1983; Heide, 1983; Lehmann, 1994), *Musca* (Egelhaaf, 1989; Heide, 1975) and *Calliphora* (Balint and Dickinson, 2001; Heide, 1971a; Heide, 1971b; Nachtigall and Wilson, 1967). However, in the past, reports of conflicting wing trajectories in flying flies generated some confusion in the field of insect flight since flies change kinematics when flown under tethered conditions compared to free flight and in response to changing wind conditions (Fry et al., 2003; Heisenberg and Wolf, 1984; Zanker, 1990b). For example, wing motion was reconstructed in freely flying *Drosophila*, *Calliphora* and *Simulium* (Ennos, 1989), in tethered *Drosophila* (Zanker, 1990a), in several species of tethered *Muscina* (Hollik, 1940) and in tethered *Phormia* (Nachtigall, 1966); and the wing tip path in tethered *Calliphora* (Wood, 1970).

Comparatively few authors, by contrast, have directly addressed the changes in wing tip trajectory during steering behaviour. Reconstructions of wing motion in a complete stroke cycle, for example, have shown that in response to optomotor stimulation, tethered flying fruit flies *Drosophila* slightly vary wing tip trajectory during yaw and roll but not excessively during pitch manoeuvres (Zanker, 1990b). Similar changes in wing tip trajectory of *Drosophila* were also observed during electrical stimulation of the second basalare control muscle (M.b2) (Lehmann, 1994). More pronounced changes in kinematics were reported in tethered flying *Calliphora vicina* during steering behaviour (Balint and Dickinson, 2001; Tu and Dickinson, 1996). While the latter insect apparently prefers a figure-eight stroke shape when M.b2 is inactive, some animals change wing trajectory towards an oval shape when M.b2 is active in order to increase stroke amplitude during course control. However, it is not clear whether in freely flying blowflies these changes are produced during clap-and-fling wing beat because in tethered calliphorid flies a full clap-and-fling sequence is apparently absent (Nachtigall, 1979). In sum, due to the lack of elaborate experimental data for kinematic changes in wing motion during clap-and-fling wingbeat in freely flying insects, it is difficult to precisely evaluate the importance of the 17 tested kinematic patterns for the control of forces and moments including power loading in an insect. Consequently, the present study highlights fundamental questions of aerodynamic force production during wing–wing interaction at various stroke kinematics rather than testing the effect of specific kinematic patterns measured during manoeuvring flight in a single insect.

Clap-and-fling lift augmentation and changes in pitch moment

Given the constraints on circulation development and endurance during clap-and-fling in real fluids, it seems evident that although total lift enhancement is modest, the clap-and-fling is a useful mechanism by which an insect can elevate force production. The data in Table 1 show that this benefit depends on the wing's heaving rate, varying between 1.4% and 17% mean lift production at 160° stroke amplitude. Since large insects employ clap-and-fling kinematics while carrying loads (Marden, 1987), or performing power demanding flight turns (Cooter and Baker, 1977), Ellington (Ellington, 1984a) thus suggested that the lacewing primarily uses clap-and-fling induced forces and moments for stability and flight control. Given the short time over which fling-induced forces act and the favourable moment arm for pitch during dorsal stroke reversal, most of the 17 tested kinematic patterns indeed produce strong nose-down pitching moments due to dorsal wing–wing interaction. Due to the complex temporal distribution of forces throughout the entire stroke cycle, however, pitching moments are not exclusively controlled by changes in vertical force during fling but are also balanced by the small attenuations in vertical force production during the wing's upstroke (Fig. 8B). The situation is even more complex, because the moment arm for pitching changes throughout the stroke cycle according to stroke and heaving angle. Thus kinematic patterns exhibiting similar mean vertical force augmentation may produce different amounts of mean pitching augmentation. For example, consider that the three kinematic patterns F, J and Q, all enhance vertical force on average by 28.5±1.3 mN, while the increase in pitching moment due to clap-and-fling is 1.51 Nmm (pattern F), –0.05 Nmm (J) and 2.35 Nmm (Q) with respect to the one-wing flapping condition. The relevance of this example is twofold. It shows, first, that the induction of pitching moments *via* clap-and-fling strongly depends on wing tip path, and second, that an insect may even modestly boost lift production without extensively changing its pitching moments. Eventually, we should remember that besides vertical forces, our analytical model also suggests that horizontal forces may contribute substantially to pitching moments and concomitant changes in instantaneous horizontal forces augmentation might conspicuously help or hinder the insect to control total pitching balance during free flight.

Significance of heaving motion for force enhancement

Linear regression analysis on the various measures suggests that vertical force augmentation decreases with increasing performance of a single flapping wing (Fig. 4A, Table 2) but is independent from rotational effect (Fig. 4C, Table 2). The latter result is somewhat surprising, because (i) total force augmentation due to clap-and-fling significantly increases with rotational force production of a single wing (Table 2), (ii) rotational timing and speed are similar among all tested kinematic patterns, and (iii) several studies have already proved the significance of wing rotation for force enhancement (Dickinson et al., 1999; Sane and Dickinson, 2002). As an alternative explanation for the changes in vertical force augmentation we hypothesize that the direction of heaving motion during clap-and-fling predominately determines the magnitude of vertical force augmentation rather than the strength of rotational effect. This approach was fuelled by the idea that downward heaving motion during fling might reinforce leading edge vortex (LEV) induction by increasing the pressure difference between the zone of the opening gap and the surrounding fluid, and thus increases lift (Fig. 9A,B). In comparison, we hypothesize that upward heaving motion during fling attenuates the negative pressure in the gap, because the wings move into the opposite direction of the fluid inflow. In other words: the wing's own vertical motion might either reinforce (downward motion) or attenuate (upward motion) the velocity of the fluid moving into the opening cleft and might thus either improve or delay LEV induction, respectively. To verify this concept, we employed three strategies: (i) analytically modelling the flow speed into the opening cleft during fling, (ii) analysing the dependency between heaving rate and lift augmentation, and (iii) sorting the kinematic patterns into two groups, according to their heaving motion during fling (downstroke heaving-up and downstroke heaving-down).

According to Weis-Fogh's original description of the clap-and-fling (Weis-Fogh, 1973), we modelled fling motion assuming a constant rate of change in angle of wing incidence.

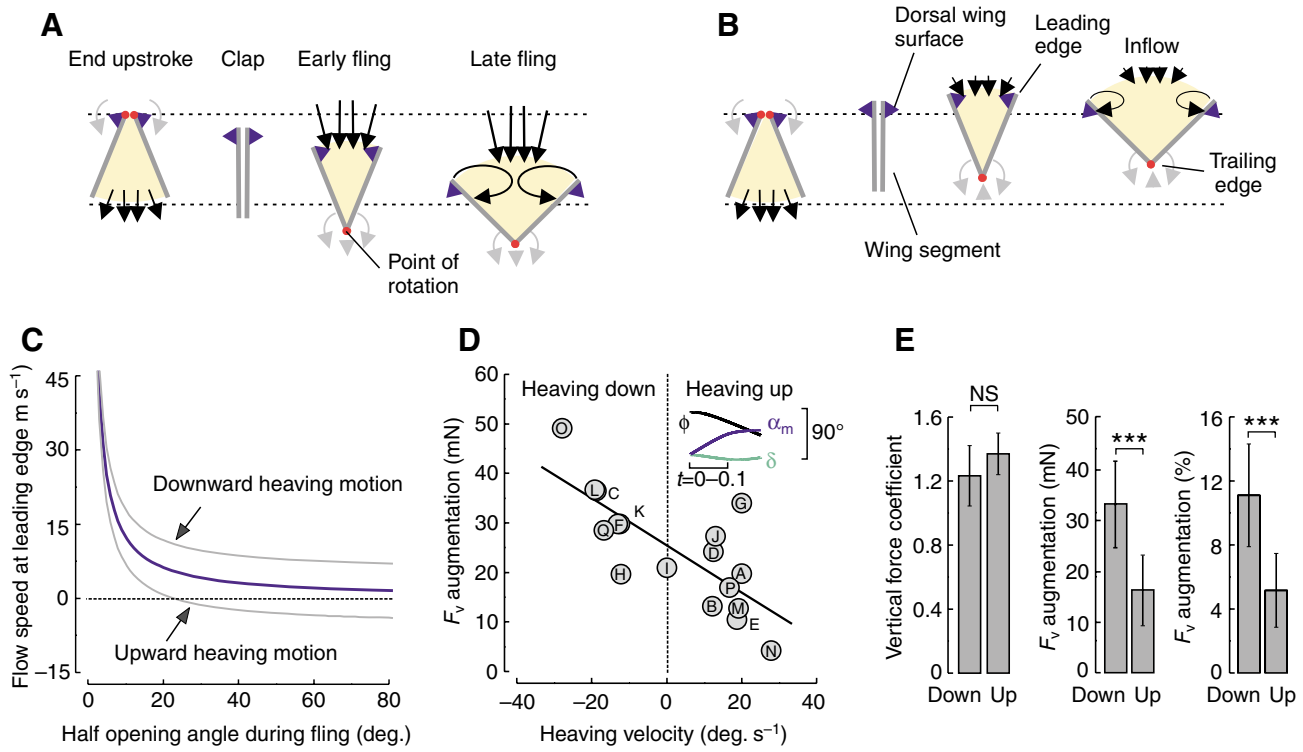

Fig. 9. Schematic reconstruction of wake pattern during wing–wake interaction in fruit fly model wings and effect of heaving motion during clap-and-fling. (A,B) The graphs show chordwise wing segments during clap-and-fling at the end of the upstroke, during the clap, and during the fling phase before the two wings separate for the downstroke. The low-pressure region evolving between the wings during the fling pulls fluid around the leading and the trailing wing edge into the opening cleft. Inflow of fluid during fling potentially increases during heaving down motion, as shown in A, and decreases when the wings move upwards at the beginning of the downstroke, as shown in B (cf. length of black straight arrows). (C) Simplified hypothetical analytical simulation modelling the inflow velocity between both leading wing edges during fling. Angular velocity during dorsal wing rotation and wing size are taken from a tethered flying fruit fly. The model predicts a reduction in flow velocities into the opening cleft during upward heaving motion whereas flow velocity increases during downward heaving compared to a wing beat without heaving motion (blue). (D) Heaving rate and direction plotted against vertical force augmentation during clap-and-fling wing beat. Pictogram illustrates the change in stroke angle (ϕ, black), the wing's angle of attack (α_m, blue) and heaving angle (δ, green). Heaving rate was derived from the angular change within a time window of 0.1 stroke cycle after the wing has started the downstroke. (E) Effect of heaving up and down motion during fling on vertical force coefficient of a single wing (left), absolute vertical force augmentation when flapping both wings (middle) and relative vertical force augmentation due to clap-and-fling (right). NS, not significant; ***P<0.001 significance level.

Additionally, during fling the wing may move vertically by a distance d_y that either adds to (upward heaving motion) or subtracts a velocity differential from flow velocity between the leading wing edges. We thus expressed velocity u_{LE} between the two leading edges, u_{LE}, by the following equation:

$$u_{LE} = 2\bar{c}\theta(\mathrm{d}\theta/\mathrm{d}t + d_y/\mathrm{d}t)\,, \qquad (16)$$

in which $\bar{c}$ is mean wing chord of the wing, the parameter θ is the total gap angle of the opening cleft and t is time (s). Angular velocity during wing rotation and wing size ($\bar{c}$=1.5 mm) were adopted from a kinematic analysis on tethered fruit flies *Drosophila virilis* flying at 150 Hz stroke frequency (F.-O.L., unpublished data). The example in Fig. 9C shows how the flow speed, passing through an arc produced by the motion of the two leading edges, changes with increasing opening angle. Without heaving motion, the flow is always directed into the cleft, as shown previously (blue, Fig. 9C) (Lehmann et al., 2005; Maxworthy, 1979; Spedding and Maxworthy, 1986). However, adding a constant upward heaving motion of one wing chord per 45° wing rotation, inflow velocity apparently reverses direction at approximately 20° opening angle, while downward heaving motion apparently reinforces absolute flow velocity and thus, supposedly, leading edge vortex induction. Fig. 9D superficially confirms the outcome of our simple analytical prediction suggesting that kinematic patterns yielding downward heaving motion produce higher vertical force augmentation due to clap-and-fling compared to kinematic patterns exhibiting upward heaving motion (linear regression fit, y=25.5–0.48x, R^2=0.57, P<0.001, N=17).

We further summarized our findings by sorting the kinematic patterns into two groups, according to their heaving motion during fling (downstroke heaving-up and downstroke heaving-down) that yielded mean vertical force augmentation of 5.16±2.31 and 11.1±3.21%, respectively (N=8 patterns, Fig. 9E). The statistical analysis suggests that vertical force

augmentation of the 'heaving-up' group (kinematic patterns, A,B,D,E,J,M,N,P) is significantly lower (ANOVA, $P<0.001$) than the value of the group with downward heaving motion (patterns C,F,G,H,K,L,O,Q), although vertical force coefficient in both groups is similar at $P=0.001$ (heaving down: $\overline{C_{F(V)}}=1.23\pm0.18$, heaving up: $\overline{C_{F(V)}}=1.37\pm0.15$, ANOVA, Fig. 9E). In conclusion, our experiments suggest that even relatively small changes in vertical heaving motion of $\pm20^\circ\ s^{-1}$ occurring during the initial part of the downstroke may account for more than a twofold change in clap-and-fling lift augmentation. Although the underlying fluid dynamic mechanisms still have to be investigated in greater detail, lift production is likely to be altered predominantly by the expected changes in flow velocity at the leading edge and thus the changes in leading edge vortex induction during fling motion.

Conclusions

The results of our experiments on the relationship between dorsal clap-and-fling effect and wing tip path have highlighted an unexpected complexity of modifications in flight force and rotational moments throughout the entire stroke cycle. Our data apparently show that heaving motion, besides many other modifications in wing kinematics, may have a pronounced impact on the effect of dorsal wing–wing interaction. Notwithstanding the limits of our approach such as the lack of wing elasticity and adequate wing surface structure, the near-clap condition, and the choice of the selected kinematic pattern, our data suggest that clap-and-fling vertical force enhancement is most beneficial in wing kinematics producing low mean vertical force coefficient during wing flapping. In insects that are limited by aerodynamic lift rather than by mechanical power of the flight musculature, we thus assume that clap-and-fling lift enhancement might be at the lower end of the values reported here, because these insects presumably maximize their performance even in the absence of clap-and-fling. In this respect, insects that rely on fast manoeuvres and high stability might benefit more strongly from a high relative increase in vertical force augmentation. Our data imply that clap-and-fling induced vertical force does not necessarily entail a concomitant strong change in nose-down pitching moment, potentially offering an insect the ability to decouple pitch from force, and thus thrust from lift control. Another hypothesis for the use of clap-and-fling wing beat in insects is that of flight power and efficiency. While lift to counterbalance gravity may be changed only moderately, power loading and propeller efficiency may change considerably during clap-and-fling wing beat due to the increase in fling-induced lift production near pronation. At this time the wing is moving relatively slowly and because profile power depends on the cube of wing velocity, the clap-and-fling manoeuvre might help to reduce power requirements and thus lowers metabolic activity in the flying animal. If this explanation holds true, however, why clap-and-fling wing beat is not a common feature in flapping flight and continuously used by flying insects still remains an open question.

List of symbols and abbreviations

$\overline{A_F}$	mean total force augmentation
$\overline{A_{F(H)}}$	mean horizontal force augmentation
$\overline{A_{F(V)}}$	mean vertical force augmentation
$\overline{A_{T(P)}}$	mean pitch moment augmentation
$\overline{C_F}$	mean total force coefficient
$\overline{C_{F(H)}}$	mean horizontal force coefficient
$\overline{C_{F(V)}}$	mean vertical force coefficient based on $\overline{F_v}$
COF	centre of force production
COG	centre of mass of the animal
$(d\hat{\delta}/d\hat{t})^2$	instantaneous square of dimensionless angular vertical wing velocity
$(d\hat{\phi}/d\hat{t})^2$	instantaneous square of dimensionless angular horizontal wing velocity
d	distance between wing hinge and centre of mass
$\hat{d}$	distance between wing hinge and centre of mass normalized to wing length
d_x, d_y, d_z	horizontal/vertical/z direction distance between wing hinge and centre of body mass
dl_x, dl_y	moment arms in horizontal and vertical direction
F	mean total force
$\overline{F_h}$	mean horizontal force of a single wing
$\overline{F_{rot}}$	mean force due to wing rotation and wake capture
$\overline{F_v}$	mean vertical force of a single wing
F_v, F_r, F_h	vertical/radial/horizontal aerodynamic force
LEV	leading edge vortex
n	stroke frequency
R	wing length
$\hat{r}_2^2(S)$	non-dimensional radius of the second moment of wing area
S	surface area of one wing
$\hat{t}$	normalized time of stroke cycle (0–1), starting with downstroke
$\overline{T_P}$	mean moment around pitch axis
U_{LE}	velocity between two leading edges
α_m	angle of attack
χ	body angle
δ	positional angle of wing in the vertical (heave angle)
ϕ	positional angle of wing in the stroke plane
Φ	stroke amplitude
γ	inclination of mean force vector with respect to the horizontal
ρ	density of air
$\hat{\psi}^2$	dimensionless horizontal and vertical angular wing velocity

We would like to acknowledge Ursula Seifert for critically reading the manuscript and the two anonymous referees for their useful comments. This work was funded by German Federal Ministry for Education and Research (BMBF) grant Biofuture 0311885 to F.-O.L.

References

Balint, C. N. and Dickinson, M. H. (2001). The correlation between wing kinematics and steering muscle activity in the blowfly *Calliphora vicina*. *J. Exp. Biol.* **204**, 4213-4226.

Bennett, L. (1977). Clap-and-fling aerodynamics – an experimental evaluation. *J. Exp. Biol.* **69**, 261-272.

Birch, J. M. and Dickinson, M. H. (2001). Spanwise flow and the attachment of the leading-edge vortex on insect wings. *Nature* **412**, 729-733.

Brackenbury, J. (1990). Wing movements in the bush cricket *Tettigonia viridissima* and the mantis *Ameles spallanziana* during natural leaping. *J. Zool. Lond.* **220**, 593-602.

Brackenbury, J. (1991a). Kinematics of take-off and climbing flight in butterflies. *J. Zool. Lond.* **224**, 251-270.

Brackenbury, J. (1991b). Wing kinematics during natural leaping in the mantids *Mantis religiosa* and *Iris oratoria*. *J. Zool. Lond.* **223**, 341-356.

Brodsky, A. K. (1991). Vortex formation in the tethered flight of the peacock butterfly *Inachis io* L. (Lepidoptera, Nymphalidae) and some aspects of insect flight evolution. *J. Exp. Biol.* **161**, 77-95.

Brodsky, A. K. (1994). *The Evolution of Insect Flight*. Oxford: Oxford University Press.

Cooter, R. J. and Baker, P. S. (1977). Weis-Fogh clap-and-fling mechanism in *Locusta*. *Nature* **269**, 53-54.

Dalton, S. (1975). *Borne on the Wind*. New York: Reader's Digest Press.

David, C. T. (1978). The relationship between body angle and flight speed in free flying *Drosophila*. *Physiol. Entomol.* **3**, 191-195.

Dickinson, M. H., Lehmann, F.-O. and Sane, S. (1999). Wing rotation and the aerodynamic basis of insect flight. *Science* **284**, 1954-1960.

Edwards, R. H. and Cheng, H. K. (1982). The separation vortex in the Weis-Fogh circulation-generation mechanism. *J. Fluid Mech.* **120**, 463-473.

Egelhaaf, M. (1989). Visual afferences to flight steering muscles controlling optomotor responses of the fly. *J. Comp. Physiol. A* **165**, 719-730.

Ellington, C. P. (1975). Non-steady-state aerodynamics of the flight of *Encarsia formosa*. In *Swimming and Flying in Nature*, Vol. 2 (ed. T. Y. Wu, C. J. Brokaw and C. Brennen), pp. 783-796. New York: Plenum Press.

Ellington, C. P. (1984a). The aerodynamics of insect flight. III. Kinematics. *Proc. R. Soc. Lond. B Biol. Sci.* **305**, 41-78.

Ellington, C. P. (1984b). The aerodynamics of insect flight. VI. Lift and power requirements. *Philos. Trans. R. Soc. Lond. B Biol. Sci.* **305**, 145-181.

Ellington, C. P. (1984c). The aerodynamics of insect flight. II. Morphological parameters. *Philos. Trans. R. Soc. Lond. B Biol. Sci.* **305**, 17-40.

Ennos, A. R. (1989). The kinematics and aerodynamics of the free flight of some Diptera. *J. Exp. Biol.* **142**, 49-85.

Fry, S. N., Sayaman, R. and Dickinson, M. H. (2003). The aerodynamics of free-flight maneuvers in *Drosophila*. *Science* **300**, 495-498.

Götz, K. G. (1983). Bewegungssehen and Flugsteuerung bei der Fliege *Drosophila*. In *BIONA-report 2* (ed. W. Nachtigall), pp. 21-34. Stuttgart: Fischer.

Götz, K. G. (1987). Course-control, metabolism and wing interference during ultralong tethered flight in *Drosophila melanogaster*. *J. Exp. Biol.* **128**, 35-46.

Heide, G. (1971a). Die Funktion der nicht-fibrillären Flugmuskeln bei der Schmeißfliege *Calliphora*. Teil I: Lage, Insertionsstellen und Innervierungsmuster der Muskeln. *Zool. Jb. Physiol.* **76**, 87-98.

Heide, G. (1971b). Die Funktion der nicht-fibrillären Flugmuskeln bei der Schmeißfliege *Calliphora*. Teil II: Muskuläre Mechanismen der Flugssteuerung und ihre nervöse Kontrolle. *Zool. Jb. Physiol.* **76**, 99-137.

Heide, G. (1975). Properties of a motor output system involved in the optomotor response in flies. *Biol. Cybern.* **20**, 99-112.

Heide, G. (1983). Neural mechanisms of flight control in Diptera. In *BIONA-report 2* (ed. W. Nachtigall), pp. 35-52. Stuttgart: Fischer.

Heisenberg, M. and Wolf, R. (1984). *Vision in Drosophila*. Berlin: Springer-Verlag.

Hollick, F. S. J. (1940). The flight of the dipterous fly *Muscina sabulans* Fallén. *Philos. Trans. R. Soc. Lond. B Biol. Sci.* **230**, 357-390.

Lehmann, F.-O. (1994). Aerodynamische, kinematische und elektrophysiologische Aspekte der Flugkrafterzeugung und Flugkraftsteuerung bei der Taufliege *Drosophila melanogaster*. PhD thesis, Max-Planck-Institute for Biological Cybernetics, University of Tübingen, Tübingen, Germany.

Lehmann, F.-O. (2004). The mechanisms of lift enhancement in insect flight. *Naturwissenschaften* **91**, 101-122.

Lehmann, F.-O. and Dickinson, M. H. (1998). The control of wing kinematics and flight forces in fruit flies (*Drosophila* spp.). *J. Exp. Biol.* **201**, 385-401.

Lehmann, F. O., Sane, S. P. and Dickinson, M. H. (2005). The aerodynamic effects of wing-wing interaction in flapping insect wings. *J. Exp. Biol.* **208**, 3075-3092.

Lighthill, M. J. (1973). On the Weis-Fogh mechanism of lift generation. *J. Fluid Mech.* **60**, 1-17.

Magnan, A. (1934). *Le vol des insectes: La locomotion chez les animaux, Vol. 1*. Paris: Hermann et Cie.

Marden, J. H. (1987). Maximum lift production during take-off in flying animals. *J. Exp. Biol.* **130**, 235-258.

Marey, E. J. (1873). *La Machine Animale*. Paris: G. Balliliere.

Maxworthy, T. (1979). Experiments on the Weis-Fogh mechanism of lift generation by insects in hovering flight. Part 1. Dynamics of the 'fling'. *J. Fluid Mech.* **93**, 47-63.

Maybury, W. J. and Lehmann, F.-O. (2004). The fluid dynamics of flight control by kinematic phase lag variation between two robotic insect wings. *J. Exp. Biol.* **207**, 4707-4726.

Miller, L. A. and Peskin, C. S. (2005). A computational fluid dynamics of 'clap-and-fling' in the smallest insects. *J. Exp. Biol.* **208**, 195-212.

Nachtigall, W. (1966). Die Kinematik der Schlagflügelbewegungen von Dipteren. Methodische und Analytische Grundlagen zur Biophysik des Insektenflugs. *Z. Vergl. Physiol.* **52**, 155-211.

Nachtigall, W. (1979). Rasche Richtungsänderungen und Torsionen schwingender Fliegenflügel und Hypothesen über zugeordnete instationäre Strömungseffekte. *J. Comp. Physiol. A* **133**, 351-355.

Nachtigall, W. and Wilson, D. M. (1967). Neuro-muscular control of dipteran flight. *J. Exp. Biol.* **47**, 77-97.

Ramamurti, R. and Sandberg, W. C. (2001). Computational study of 3-D flapping foil flows. *39th Aerospace Sciences Meeting and Exhibit*, 605.

Sane, S. (2003). The aerodynamics of insect flight. *J. Exp. Biol.* **206**, 4191-4208.

Sane, S. and Dickinson, M. H. (2001). The control of flight force by a flapping wing: lift and drag production. *J. Exp. Biol.* **204**, 2607-2626.

Sane, S. and Dickinson, M. H. (2002). The aerodynamic effects of wing rotation and a revised quasi-steady model of flapping flight. *J. Exp. Biol.* **205**, 1087-1096.

Schneider, P. (1980). Beiträge zur Flugbiologie der Käfer 5. Kinematik der Alae und vertikale Richtungsänderung. *Zool. Anz.* **3/4**, 188-198.

Spedding, G. R. and Maxworthy, T. (1986). The generation of circulation and lift in a rigid two-dimensional fling. *J. Fluid Mech.* **165**, 247-272.

Sun, M. and Yu, X. (2003). Flows around two airfoils performing fling and subsequent translation and translation and subsequent clap. *Acta Mech. Sinica* **19**, 103-117.

Sunada, S., Kawachi, K., Watanabe, I. and Azuma, A. (1993). Fundamental analysis of three-dimensional 'near fling'. *J. Exp. Biol.* **183**, 217-248.

Tu, M. S. and Dickinson, M. H. (1996). The control of wing kinematics by two steering muscles of the blowfly, *Calliphora vicina*. *J. Comp. Physiol. A* **178**, 813-830.

Vogel, S. (1966). Flight in *Drosophila.* I. Flight performance of tethered flies. *J. Exp. Biol.* **44**, 567-578.

Weis-Fogh, T. (1973). Quick estimates of flight fitness in hovering animals, including novel mechanisms for lift production. *J. Exp. Biol.* **59**, 169-230.

Wood, J. (1970). A study of the instantaneous air velocities in a plane behind the wings of certain Diptera flying in a wind tunnel. *J. Exp. Biol.* **52**, 17-25.

Zanker, J. M. (1988a). How does lateral abdomen deflection contribute to flight control of *Drosophila melanogaster*. *J. Comp. Physiol A* **162**, 581-588.

Zanker, J. M. (1988b). On the mechanism of speed and altitude control in *Drosophila melanogaster*. *Physiol. Entomol.* **13**, 351-361.

Zanker, J. M. (1990a). The wing beat of *Drosophila melanogaster* I. Kinematics. *Philos. Trans. R. Soc. Lond. B Biol. Sci.* **327**, 1-18.

Zanker, J. M. (1990b). The wing beat of *Drosophila melanogaster* III. Control. *Philos. Trans. R. Soc. Lond. B Biol. Sci.* **327**, 45-64.